Normal Fault Rupture Interaction with Strip Foundations

I. Anastasopoulos[1]; G. Gazetas, M.ASCE[2]; M. F. Bransby[3]; M. C. R. Davies[4]; and A. El Nahas[5]

Abstract: Observations after earthquakes where surface fault ruptures crossed engineering facilities reveal that some structures survived the rupture almost unscathed. In some cases, the rupture path appears to divert, "avoiding" the structure. Such observations point to an interaction between the propagating rupture, the soil, and the foundation. This paper (i) develops a two-step nonlinear finite-element methodology to study rupture propagation and its interaction with strip foundations; (ii) provides validation through successful Class "A" predictions of centrifuge model tests; and (iii) conducts a parameter study on the interaction of strip foundations with normal fault ruptures. It is shown that a *heavily* loaded foundation can substantially divert the rupture path, which may avoid outcropping underneath the foundation. The latter undergoes rigid body rotation, often detaching from the soil. Its distress arises mainly from the ensuing loss of support that takes place either at the edges or around its center. The average pressure q on the foundation largely dictates the width of such unsupported spans. Increasing q decreases the unsupported width, reducing foundation distress. The role of q is dual: (1) it compresses the soil, "flattening" fault-induced surface "anomalies"; and (2) it changes the stress field underneath the foundation, facilitating rupture diversion. However, even if the rupture is diverted, the foundation may undergo significant stressing, depending on its position relative to the fault outcrop.

DOI: 10.1061/(ASCE)1090-0241(2009)135:3(359)

CE Database subject headings: Geological faults; Soil-structure interaction; Finite element method; Centrifuge models; Seismic effects; Foundations.

Introduction

Seismic codes and engineering practice had in the past invariably demanded "buildings and important structures not be erected in the immediate vicinity of active faults" (Eurocode EC8 1994). Such a strict prohibition is difficult (and sometimes meaningless) to obey for a number of reasons. First, it is usually difficult to infer reliably which of the numerous geologic faults encountered in engineering practice is potentially active. Especially for long structures, such as bridges and tunnels, which often cannot avoid crossing such faults, the question of their potential activity often culminates into a hotly debated unresolvable issue. Even when the fault and its seismic activity are well defined, the prediction of the exact location of fault outcropping is not at all straightforward.

The likelihood, position, and magnitude of a surface fault emergence depend not only on the type and magnitude of the fault rupture, but also on the geometry and material characteristics of the overlying soil. Field observations (Slemmons 1957; Brune and Allen 1967; Taylor et al. 1985; Ambraseys and Jackson 1984; Kelson et al. 2001) and analytical and experimental research findings (Sanford 1959; Horsfield 1977; Roth et al. 1981; Cole and Lade 1984; Bray 1990; Bray et al. 1994a,b; Bray 2001; Johansson and Konagai 2004; Anastasopoulos et al. 2007) show that deep and "ductile" soil deposits may mask a small fault rupture, whereas by contrast with a shallow and/or "brittle" soil deposit, a large offset in the base rock will develop a distinct surface fault scarp of almost the same displacement.

Most importantly, the presence of a structure on top of the soil deposit may further modify the path of the rupture, as the latter propagates from the base rock to the ground surface. Depending on the rigidity of the foundation and the transmitted weight of the superstructure, even complete diversion of the fault path may take place (Berill 1983). The damage to a structure depends not only on its position relative to the fault outcrop in the "free-field," but also on whether and by how much such a diversion may occur. An interaction develops between the propagating rupture, the deforming soil, and the foundation-structure system. This interaction is of profound significance for the performance of a structure, and is named hereafter "fault rupture-soil foundation structure interaction" (FR-SFSI).

The prime objective of this paper is to explore the role of this interaction, numerically and experimentally. To this end:

1. A two-step nonlinear finite-element (FE) methodology is developed to study fault rupture propagation through soil and its interaction with strip foundations. The propagation of the fault rupture in the "free-field" is studied in the first step; the interaction between the outcropping dislocation and the foundation in the second.
2. The developed FE analysis method is validated through successful Class "A" predictions (Lambe 1973) of centrifuge model tests conducted in the University of Dundee, Scotland.

[1]Postdoctoral Researcher, National Technical Univ., Athens, 15780 Zografou, Greece.

[2]Professor, National Technical Univ., Athens, 15780 Zografou, Greece.

[3]Senior Lecturer, Univ. of Dundee, Nethergate, Dundee DD1 4HN, Scotland, U.K.

[4]Professor, Univ. of Auckland, New Zealand; formerly, Univ. of Dundee, Nethergate, Dundee DD1 4HN, Scotland, U.K.

[5]Formerly, Postdoctoral Researcher, Univ. of Dundee, Nethergate, Dundee DD1 4HN, Scotland, U.K.

Note. Discussion open until August 1, 2009. Separate discussions must be submitted for individual papers. The manuscript for this paper was submitted for review and possible publication on January 23, 2007; approved on May 29, 2008. This paper is part of the ***Journal of Geotechnical and Geoenvironmental Engineering***, Vol. 135, No. 3, March 1, 2009. ©ASCE, ISSN 1090-0241/2009/3-359–370/$25.00.

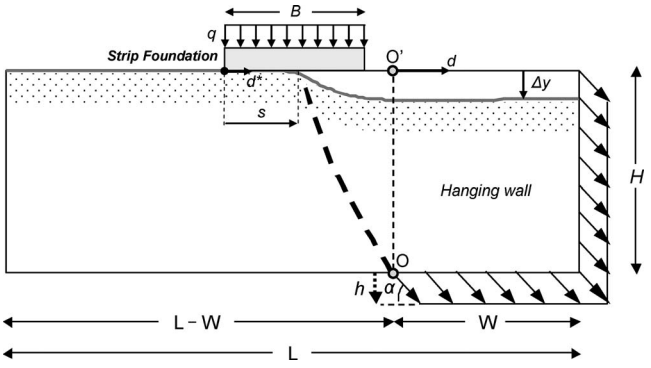

Fig. 1. Problem definition and model dimensions: interaction of fault rupture with strip foundation of width B subjected to uniform load q; the left edge of the foundation is at distance s from the point of dislocation outcropping in the free field

3. The validated FE method is utilized in conducting a parametric study on the interaction of strip foundations with a normal fault rupture.

Problem Definition

The problem studied herein is illustrated in Fig. 1. We consider a uniform soil deposit of thickness H at the base of which a normal fault, dipping at angle α (measured from the horizontal), produces downward displacement of vertical amplitude h. The analysis is conducted in two steps. First, fault rupture propagation through soil is analyzed in the free field, ignoring the presence of the structure. A strip foundation of width B carrying a uniformly distributed load q is then placed at a prespecified distance s from the free-field fault outcrop, and the analysis of the soil-structure system is performed. Both analyses are conducted under 2D plane-strain conditions. The same procedure was applied for the centrifuge model tests. While the first step (free-field fault rupture propagation) has been reported in Anastasopoulos et al. (2007), this paper focuses on the second step (i.e., the interaction with strip footings).

Finite-Element Modeling Methodology

Published research has shown that both the FE method (Bray et al. 1994a,b) and the finite difference method (Walters and Thomas 1982; White et al. 1994; Nakai et al. 1995) can be successful in simulating fault rupture propagation through soil. A necessary prerequisite is the adoption of a refined mesh (Bray 1990) and of an appropriate constitutive model of soil. Following the findings of a thorough literature review, an elastoplastic constitutive model with Mohr-Coulomb failure criterion and isotropic strain softening was adopted and encoded in the ABAQUS (2004) FE environment. Strain softening is introduced by reducing the mobilized friction angle φ_{mob} and the mobilized dilation angle ψ_{mob} with the increase of plastic octahedral shear strain

$$\varphi_{mob} = \begin{Bmatrix} \varphi_p - \dfrac{\varphi_p - \varphi_{res}}{\gamma_f^P}\gamma_{oct}^P & \text{for } 0 \leq \gamma_{oct}^P < \gamma_f^P \\ \varphi_{res} & \text{for } \gamma_{oct}^P \geq \gamma_f^P \end{Bmatrix} \quad (1)$$

$$\psi_{mob} = \begin{Bmatrix} \psi_p\left(1 - \dfrac{\gamma_{oct}^P}{\gamma_f^P}\right) & \text{for } 0 \leq \gamma_{oct}^P < \gamma_f^P \\ \psi_{res} & \text{for } \gamma_{oct}^P \geq \gamma_f^P \end{Bmatrix} \quad (2)$$

where φ_p and φ_{res}=peak mobilized friction angle and its residual (or critical state) value; ψ_p=peak dilation angle; and γ_f^P=plastic octahedral shear strain at the end of softening. To take account of scale effects (Stone and Muir Wood 1992; Muir Wood and Stone 1994; Muir Wood 2002), an approximate simplified scaling method is employed for γ_f^P, as described in Anastasopoulos et al. (2007) along with the procedure for calibration of model parameters. Preyield behavior is modeled as linear elastic, with a secant modulus $G_S = \tau_y/\gamma_y$ linearly increasing with depth.

The foundation, modeled with linear elastic beam elements, is positioned on top of the soil model and connected to it through special contact elements, which are rigid in compression but tensionless, allowing detachment of the foundation from the bearing soil (i.e., gap formation beneath the foundation). While positive normal force is transmitted, the interface shear properties follow Coulomb's friction law, allowing for slippage. Both detachment and slippage are important phenomena for realistic foundation modeling.

Free-Field Fault Rupture Propagation: Validation of the Numerical Method

The capability of the constitutive model to reproduce soil behavior has been validated through FE simulations of direct shear tests. The results of such a simulation on Fontainebleau sand have been shown to compare satisfactorily with experimental data (Gaudin 2002) in Anastasopoulos et al. (2007).

The use of strain softening models may lead to mesh dependency (Pietruszezak and Mroz 1981). Such effects have been explored in Anastasopoulos et al. (2007) through a detailed parametric study. Experimental data were utilized to judge the results from different FE meshes. The thickness of the shear zone was found to depend on mesh size d_{FE}. However, with $d_{FE} \leq 1$ m, the orientation of the propagation path and the outcropping location were not sensitive to mesh density, provided that scale similarity is maintained (through proper calibration of γ_f^P).

The consistency of the developed FE modeling methodology was first verified (Anastasopoulos 2005) through qualitative comparison with published case histories (Slemmons 1957; Brune and Allen 1967; Taylor et al. 1985) and experimental research (Horsfield 1977; Cole and Lade 1984). It was further validated through successful Class "A" predictions of centrifuge model tests of dip slip fault rupture propagation through sand in the free field (Anastasopoulos et al. 2007). These tests consisted of two normal and two reverse fault ruptures at $\alpha = 60°$ through dry medium-loose ($D_r \approx 60\%$) and medium-dense ($D_r \approx 80\%$) Fontainebleau sand. The depth of the prototype deposit was kept constant, $H = 25$ m. In all cases, the FE modeling technique predicted with accuracy both the location of fault outcropping, and the displacement profile of the ground surface.

Interaction with Strip Foundations: Validation through Centrifuge Model Tests

Centrifuge Model Configuration

A special apparatus was designed and constructed in the University of Dundee (El Nahas et al. 2006) to simulate dip slip faulting

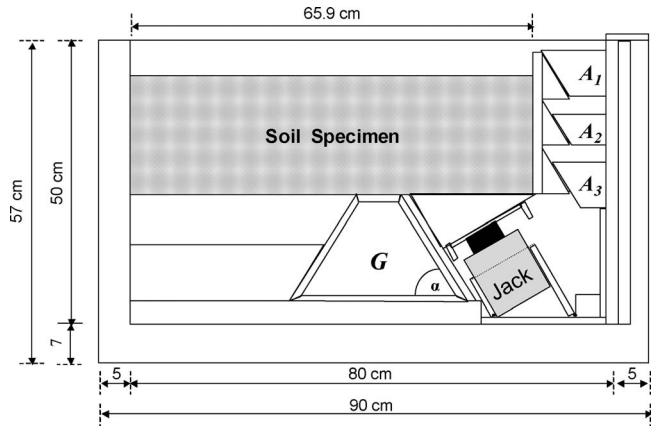

Fig. 2. Basic dimensions of the experimental apparatus developed in the University of Dundee to simulate the propagation of dip slip fault rupture through soil, and its interaction with strip foundations

and its interaction with strip foundations (Fig. 2). Two oil-driven linear actuators were used to push the right part of the apparatus up or down, simulating reverse and normal faulting, respectively. A central guidance system (G) and three aluminum wedges (A_1, A_2, and A_3) were installed to impose fault displacement at the desired α (60°). Images of the deformed soil specimen at different bedrock displacements were captured using a digital camera. Vertical and horizontal displacements at different positions within the specimen were computed through image analysis, using the Geo-PIV program (White et al. 2003), and measured directly at several points on the surface using linearly variable differential transformers (LVDTs). Displacement profiles and shear strain contours were also computed through additional postprocessing.

As previously mentioned, a series of centrifuge model tests were first conducted to investigate fault rupture propagation in the free field. Fontainebleau sand was utilized for all experiments. One such test (Test 12: normal faulting, medium-loose $D_r \approx 60\%$ sand) was then selected as the *reference* for interaction experiments: the location of fault outcropping in the free field is necessary to define the distance s (Fig. 1). For all tests, the soil sample was prepared by dry pluviation.

FE predictions were conducted for five experiments to investigate fault-footing interaction. The experiments consisted of a partial parametric study with variation of: (i) the distributed load q acting on the foundation; and (ii) the foundation position with respect to the point of free-field fault emergence. With the exception of one flexible foundation test, all foundations were practically rigid. For all tests, soil and fault conditions were kept as constant as possible ($D_r \approx 60\%$, $H \approx 25$ m, normal faulting at 60°, 115 g centrifugal acceleration).

The following combinations were analyzed:

- Test 14: $B=10$ m, $q=90$ kPa, at $s=2.9$ m.
- Test 15: $B=10$ m, $q=37$ kPa, at $s=3.0$ m.
- Test 18: $B=10$ m, $q=91$ kPa, at $s=8.1$ m.
- Test 20: $B=25$ m, $q=91$ kPa, at $s=10.5$ m.
- Test 22: $B=9.4$ m flexible foundation, $q=84$ kPa, at $s=2.8$ m.

Due to space limitations, we focus only on the results of Tests 14, 15, and 18. Numerical predictions were equally successful for the other two tests.

Fault Rupture Propagation in the Free Field (Test 12)

Before proceeding to the discussion of interaction model tests, it is necessary to summarize the results of Test 12, which is the free-field *reference* for all other tests. Model parameters were calibrated as described in Anastasopoulos et al. (2007). Specifically, the following parameters were used: $\varphi_p=34°$, $\varphi_{res}=30°$, $\psi_p=6°$, $\gamma_y=0.03$, $\gamma_p^P=0.06$, and $\gamma_f^P=0.244$. Analytical predictions are compared with centrifuge model test results in terms of: (a) deformation and shear strain localization; and (b) the vertical displacement profile of the ground surface.

Fig. 3 compares centrifuge test images and computed shear strain contours with FE deformed mesh and shear strain contours, for two levels of imposed bedrock offset. For fault throw $h=0.75$ m (experiment: $h \approx 0.79$ m), the FE analysis suggests that the rupture has just outcropped. In the experiment, the rupture (S1) has propagated by almost 2/3 of H, without, however, having emerged. Observe also that this initial rupture tends to bend slightly over the hanging wall, something not predicted in the analysis. Interestingly, the increase of h leads to the development of a less steep slip plane (S2), which is the one that finally

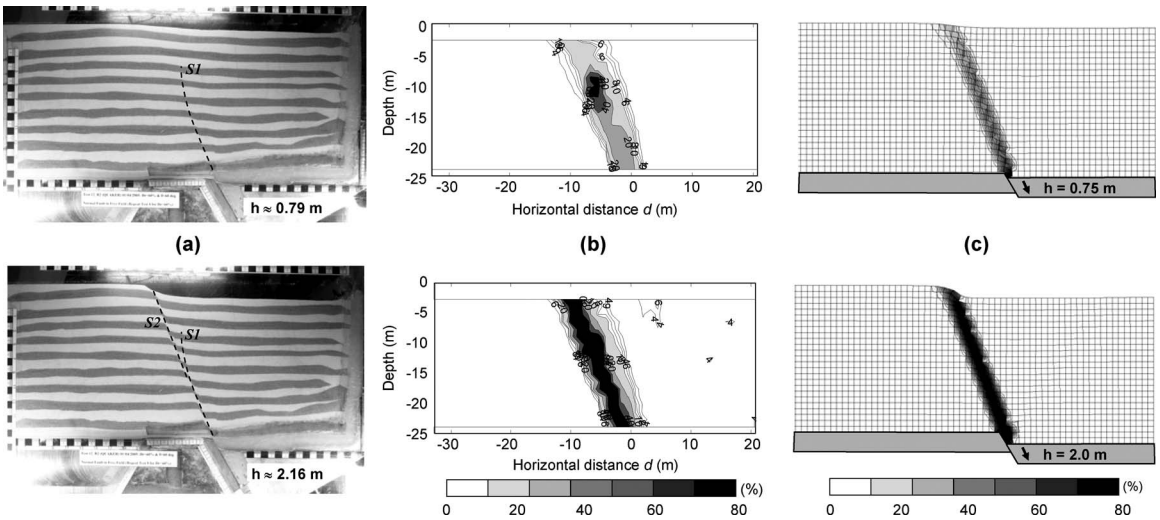

Fig. 3. Test 12—free-field fault rupture propagation through $D_r=60\%$ Fontainebleau sand ($\alpha=60°$): (a) centrifuge model test images; (b) experimental shear strain contours; and compared to (c) FE predicted deformed mesh with shear strain contours

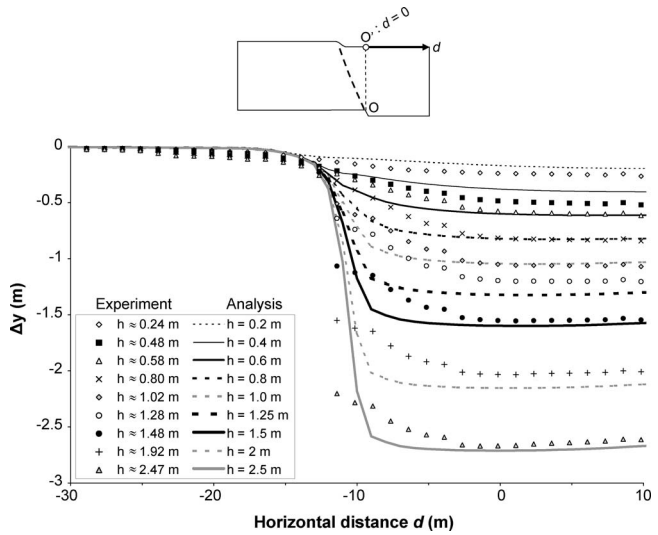

Fig. 4. Class "A" prediction of Test 12—free-field fault rupture propagation through $D_r=60\%$ Fontainebleau sand ($\alpha=60°$): comparison of numerical with experimental vertical displacement of the surface; imposed bedrock dislocation $h=0.2$ m to 2.5 m

propagates all the way to the surface. For $h=2.0$ m (experiment: $h\approx 2.16$ m), S2 has clearly outcropped and the deformation is localized in a narrow band, in accord with FE results. Experimental shear strain contours seem to be a little more diffuse than the FE prediction.

Fig. 4 illustrates the comparison in terms of vertical displacement at the surface, for $h=0.2-2.5$ m. FE analysis and experimental results agree reasonably well in the location of fault outcropping, about 10 m left from the vertical projection of the point of application of bedrock displacement, denoted O′ in Fig. 1. Surface deformation seems to be slightly more localized in the experiment, but the comparison in terms of shear zone thickness remains satisfactory. The required base h for the rupture to outcrop is also predicted reasonably well.

B=10 m Foundation, Subjected to q=90 kPa, at s=2.9 m (Test 14)

The base case of a 10 m wide foundation subjected to $q=90$ kPa is considered first. This value was selected as an upper bound pressure for buildings on mat foundations (corresponding to an approximately nine-story structure). The foundation is positioned so that the free-field fault rupture would have emerged 2.9 m from its left edge. This geometry is utilized later as a reference for the parametric investigation.

In the experiment, a secondary steep rupture zone, S1′ (practically the same as S1 of Test 12), develops and propagates half the way to the surface for $h\leq 0.48$ m (Fig. 5). In the analysis, for $h=0.5$ m, the rupture has just outcropped to the left of the foundation, diverted by about 3 m towards the footwall. While the test image does not seem to support FE results, experimental shear strain contours are in accord. For $h=2.0$ m, S1′ can be seen to be diverted slightly towards the hanging wall compared to the free-field path, S1. More importantly, a second localization (similar to S2 of Test 12), S2′, forms to the left of the foundation. This second rupture is diverted by ~3 m towards the footwall, missing the foundation.

Fig. 6(a) compares experimental with numerical results in terms of vertical displacement, Δy, at the surface, revealing satisfactory agreement for all magnitudes of h. The FE analysis predicts correctly the diversion of the rupture path to the left of the foundation. While in the free field (Test 12), the rupture outcrops at $d=-10$ m, it now emerges at $d=-13$ m. Despite the diversion, the foundation experiences measurable rotation. For $h=2.5$ m, about 0.3 m of the imposed dislocation is converted to rigid body rotation of 1.7°, while the remaining 2.2 m is localized to the left of the foundation in the form of a distinct scarp. The discrepancy between analysis and experiment near the left edge of the footing (circled in the diagram) may be attributable to inaccuracies of the digital image analysis for the centrifuge model test. It is believed that sand may have spuriously moved above the footing at the area near the window; thus, instead of a rigid surface (as correctly seen in the analysis), the experimental measurement shows curving. The remaining measurements were not affected

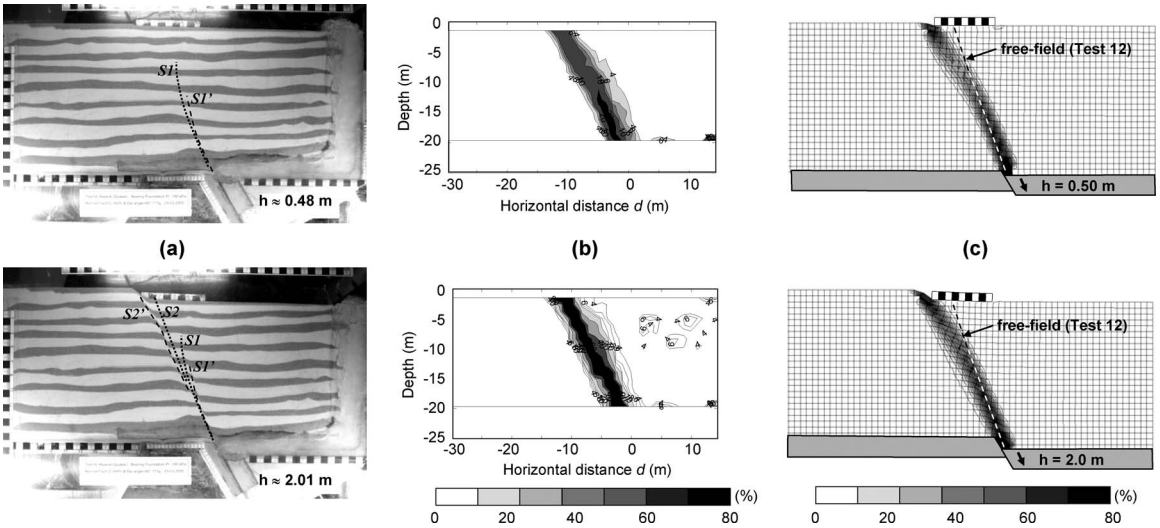

Fig. 5. Test 14—rigid foundation $B=10$ m in width, transmitting a pressure $q=90$ kPa, positioned at distance $s=2.9$ m with respect to the free-field (unperturbed) point of emergence of the fault rupture: (a) centrifuge model test images; (b) centrifuge shear strain contours; and compared to (c) FE computed deformed mesh with shear strain contours

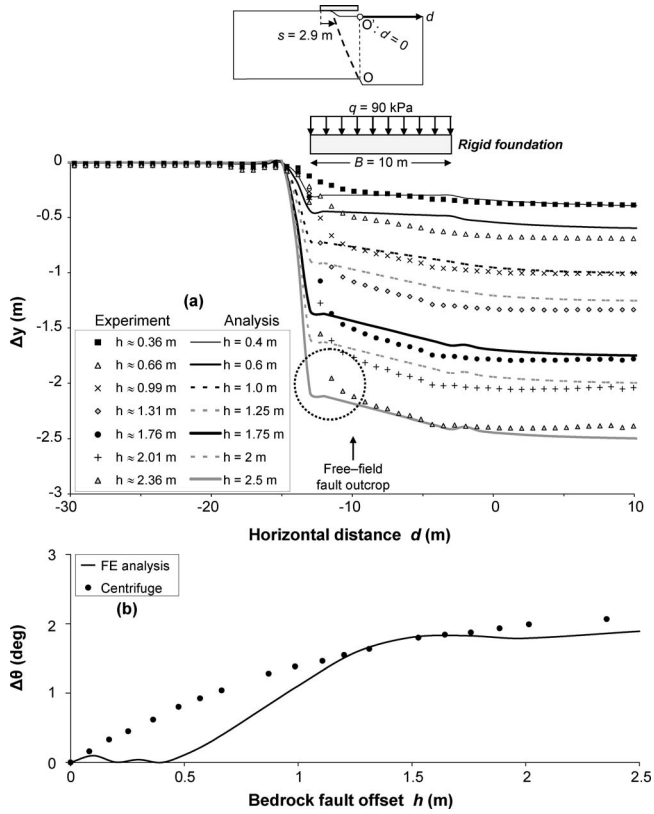

Fig. 6. Class "A" prediction of Test 14—rigid foundation $B=10$ m, $q=90$ kPa, $s=2.9$ m: (a) vertical displacement profile of the surface; (b) foundation rotation $\Delta\theta$ versus bedrock fault offset h

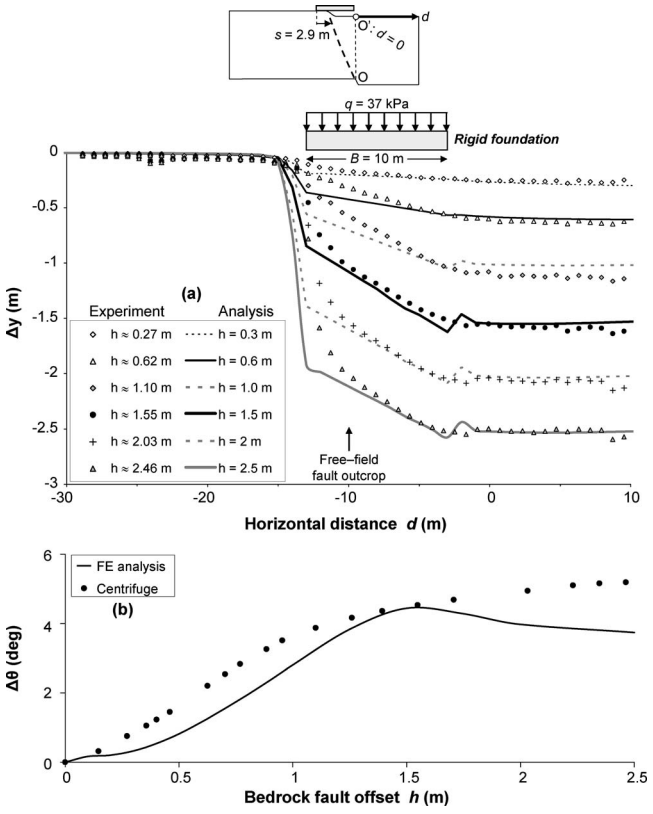

Fig. 8. Class "A" prediction of Test 15—rigid foundation, $B=10$ m, $q=37$ kPa, $s=3.0$ m: (a) vertical displacement profile of the surface; (b) foundation rotation $\Delta\theta$ versus bedrock fault offset h

by this small inaccuracy. With the exception of low imposed fault offsets ($h<1$ m), the analytical prediction is successful with respect to foundation rotation $\Delta\theta$ [Fig. 6(b)].

B=10 m Foundation, Subjected to q=37 kPa, at s=3.0 m (Test 15)

To highlight the effect of q, Test 14 was repeated, but with $q=37$ kPa (instead of 90 kPa). As illustrated in Fig. 7, the response remains qualitatively the same, with the main difference being the increase of foundation rotation. The comparison of experimental measurements with numerical Δy at the surface [Fig. 8(a)] is again quite satisfactory. The foundation now experiences larger rotation: about 0.6 m of the imposed dislocation is converted to rigid body rotation, while the remaining 1.9 m is localized to the left of the foundation. The numerical prediction

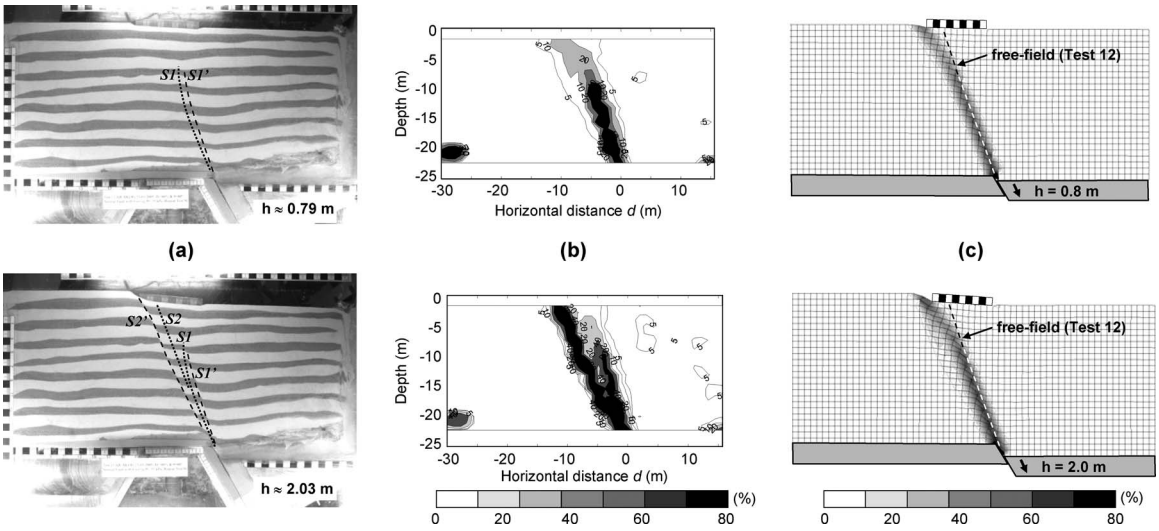

Fig. 7. Test 15—rigid foundation, $B=10$ m, transmitting a pressure $q=37$ kPa, at $s=3.0$ m: (a) centrifuge model test images; (b) centrifuge shear strain contours; and compared to (c) FE computed deformed mesh with shear strain contours

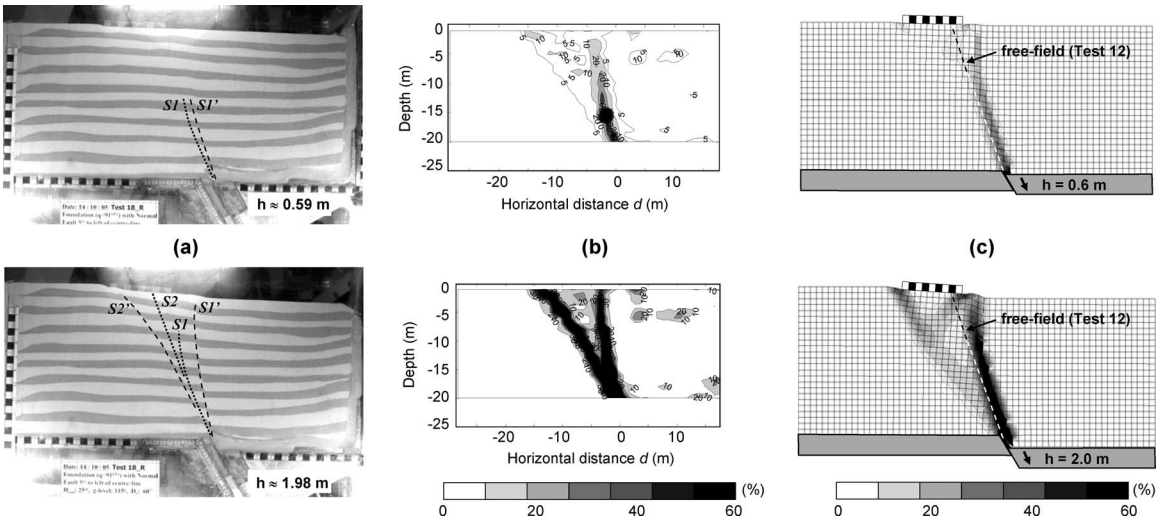

Fig. 9. Test 18—rigid foundation, $B=10$ m, transmitting a pressure $q=91$ kPa, at $s=8.1$ m: (a) centrifuge model test images; (b) centrifuge shear strain contours; and compared to (c) FE predicted deformed mesh with shear strain contours

is successful with respect to $\Delta\theta$ [Fig. 8(b)], which has almost doubled compared to the heavily loaded foundation (Test 14, $q=90$ kPa).

B= 10 m Foundation, Subjected to q= 91 kPa, at s= 8.1 m (Test 18)

To investigate the effect of position s, Test 14 was repeated with the foundation offset at $s=8.1$ m (instead of 2.9 m) relative to the free-field fault rupture emergence. For small levels of imposed deformation ($h\approx 0.59$), the response remains qualitatively the same with previous tests (Fig. 9). The difference in the interaction geometry starts being visible at larger displacements: for $h\approx 1.98$ m (analysis: $h=2.0$ m), S1′ extends all the way to the surface, where it becomes steeper and diverted towards the hanging wall by ~6 m. A second rupture S2′ makes its appearance. Strongly diverted towards the footwall, it outcrops just to the left of the foundation. Compared to its free-field equivalent, S2, it is diverted by ~8 m. Observe that: (i) in the previous tests S1′ never outcropped—with the increase of h it became kinematically inadmissible, and S2′ was the one to emerge; (ii) the diversion of S1′ is towards the hanging wall—that of S2′ is still towards the footwall; and (iii) S1′ is not just diverted to the edge of the foundation—it moves about 3 m further to the right of it. The FE analysis predicts correctly both ruptures, with the only difference being a somehow larger strain concentration on S1′.

With the exception of a 1–2 m difference in the position of emergence of S2′ the comparison is satisfactory in terms of Δy at the surface [Fig. 10(a)] and foundation rotation $\Delta\theta$ [Fig. 10(b)]. Compared to Test 14 ($s=2.9$ m), $\Delta\theta$ is substantially larger: for $h=2.0$ m, analysis and centrifuge suggest that ~0.8 m of the imposed dislocation is converted to rigid body rotation ($\Delta\theta\approx 5°$), while the remaining ~1.2 m is localized to the right of the foundation.

Parametric Study on Fault Rupture Interaction with Strip Foundations

This section summarizes the results of a parametric study on the interaction of a normal fault rupture with strip foundations. The effect of the following factors is investigated:

(a) The relative location s of the free-field fault outcrop from the left edge of the foundation; $s=1$, 3, 5, 7, and 9 m (in dimensionless form: $s/B=0.1$ to 0.9).
(b) The uniformly distributed load q acting on the foundation; $q=10$, 20, 40, and 80 kPa, i.e., roughly typical values for one-, two-, four-, and eight-story buildings.
(c) The foundation rigidity EI (where E and I=Young's modulus and the moment of inertia of the foundation); EI=10^4,

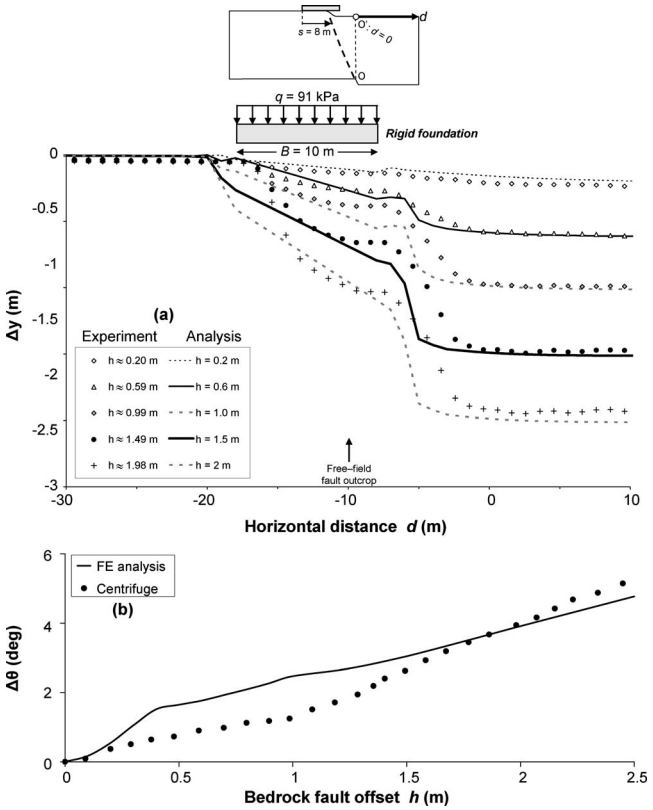

Fig. 10. Class "A" prediction of Test 18—rigid foundation, $B=10$ m, $q=91$ kPa, $s=8.1$ m: (a) vertical displacement profile of the surface; (b) foundation rotation $\Delta\theta$ versus bedrock fault offset h

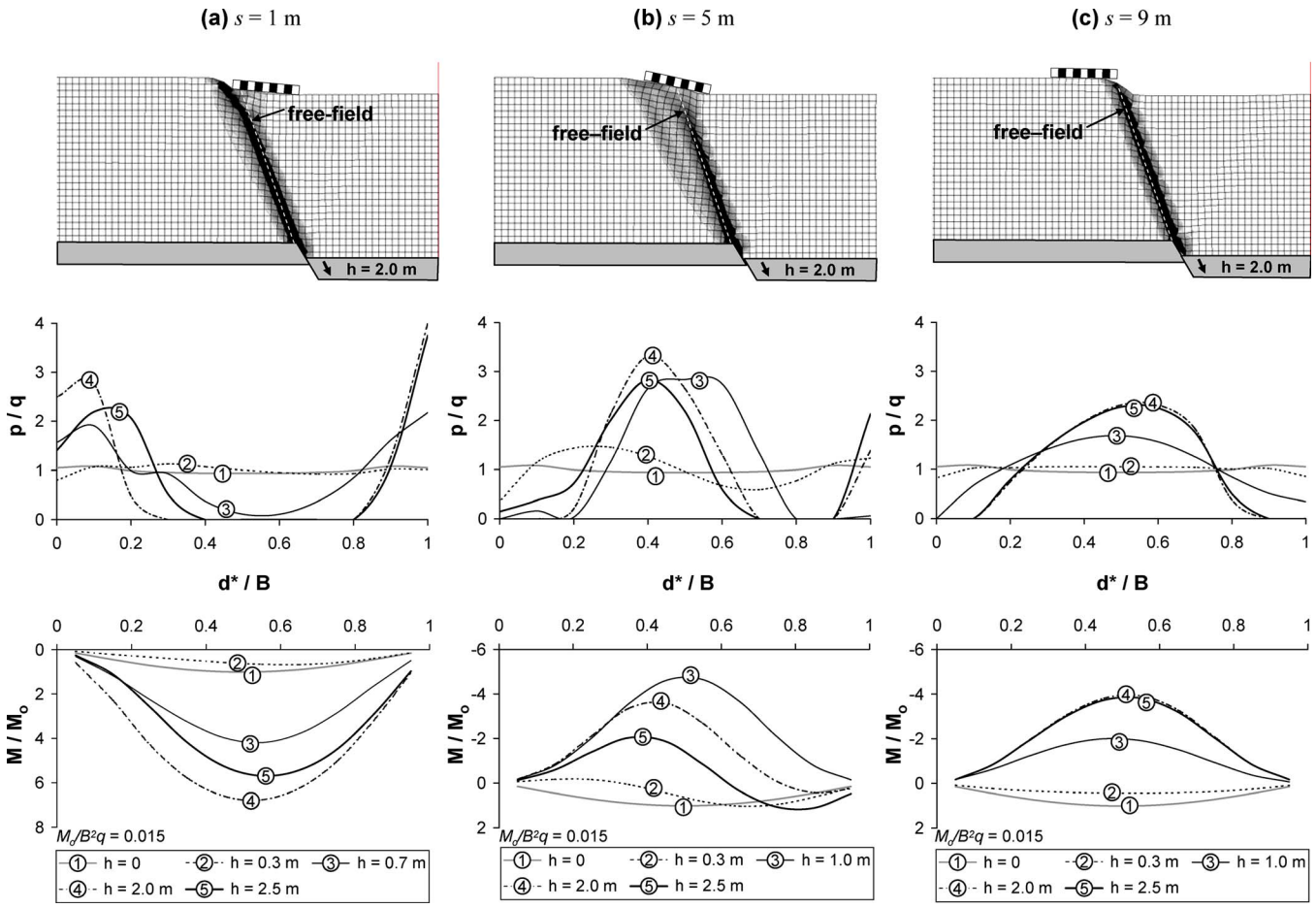

Fig. 11. Effect of relative location s; $B=10$ m, EI$=10^8$ kN m^2 foundation, transmitted load $q=20$ kPa: (a) $s=1$ m; (b) $s=5$ m; and (c) $s=9$ m; from top to bottom: deformed mesh with shear strain contours, normalized contact pressure p/q and bending moment M/M_o (M_o: maximum bending moment, at $h=0$)

10^5, 10^6, 10^7, and 10^8 kNm^2 to cover a wide range from a flexible to a practically rigid foundation.

To facilitate evaluation of the effect of the aforementioned factors, soil properties, fault dip ($\alpha=60°$), and foundation width ($B=10$ m) are held constant.

Effect of Position s

To highlight the effect of s, the response of a practically rigid (EI$=10^8$ kNm^2) $B=10$ m foundation subjected to $q=20$ kPa, is illustrated for: $s=1$, 5, and 9 m. The comparison is shown in Fig. 11 in terms of deformed mesh with shear strain contours (for $h=2.0$ m), along with the evolution of contact pressures p and foundation bending moments M with h. p is normalized with q, and M with the maximum bending moment M_o before faulting. The value of initial moment $M_o/B^2q=0.015$ is also given in the figure. The normalization with M_o is used as a direct means to show the difference of the tectonically induced distress, compared to the stressing due to the foundation loading q.

For $s=1$ m [Fig. 11(a)], the rupture is diverted toward the footwall, to the left of the foundation. Despite this diversion, the foundation experiences significant stressing. Initially, for $h=0$, the foundation is in full contact with the soil: p/q is more or less equal to 1 throughout its whole width (as long as some inelasticity reduces the elasticity spikes under the edges). For $h=0.3$ m, a minor change in the distribution of p/q can be observed: the rupture has not yet outcropped. For $h=0.7$ m, the rupture emerges to the left of the foundation, which is almost losing contact near the center ($d^*/B\approx0.5$). For $h=2.0$ m, the foundation is then detached from the soil from $d^*/B=0.3$ to 0.8; i.e., it is supported only at the two edges, from $d^*/B=0$ to 0.3 and from $d^*/B=0.8$ to 1.0. This means that the foundation tends to behave as a simply supported beam on "elastic" supports. Surprisingly, further increasing h to 2.5 m tends to close the gap, i.e., decrease the unsupported central span of the foundation. This is attributable to soil yielding near the two support edges: under high stressing, the soil starts yielding and a new equilibrium is attainable through increased supported width.

These changes in p/q are responsible for the alteration of M/M_o. Initially, for $h=0.3$ m, M/M_o is slightly reduced, indicative of bending in the opposite direction: indeed while the external load q bends the foundation downwards (sagging deformation), faulting-induced deformation initially causes upward bending (hogging deformation). However, this is true only for small values of dislocation, when the rupture does not outcrop and the soil deforms quasi-elastically. By increasing h to 0.7 m, the rupture outcrops, leading to rereversal of the stressing. Now, the foundation is again subjected to sagging deformation, induced by the detachment at its middle. Further increasing h to 2.0 m increases M/M_o to a maximum of 6.8 (i.e., the faulting

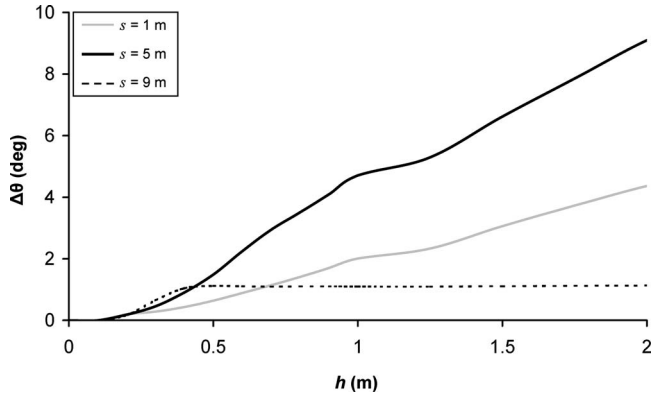

Fig. 12. Effect of relative location s on foundation rotation $\Delta\theta$ with respect to bedrock fault offset h; $B=10$ m, EI$=10^8$ kN m^2 foundation, $q=20$ kPa

induced stressing is 6.8 times the static). Finally, for $h=2.5$ m, due to the aforementioned increased area of contact, M/M_o reduces to 5.7.

The response is altered significantly with the rupture at the middle ($s=5$ m): no diversion is observed [Fig. 11(b)]. Instead, a considerable amount of plastic deformation is diffused underneath the foundation, while a secondary rupture starts propagating downwards from its left edge. Initially ($h=0.3$ m), p/q is not altered significantly. For $h=1.0$ m, the rupture then reaches the foundation, generating loss of support at the edges (from $d^*/B=0$ to 0.2, and from 0.8 to 1.0). The two unsupported spans essentially act as cantilevers on "elastic" supports. The outcome is a complete reversal of stressing, with M/M_o reaching −4.8 (the minus sign represents hogging deformation).

Increasing h to 2.0 m leads to a new equilibrium scheme. While the first "cantilever" (at the left) remains, the second one (at the right) is converted to a "simply supported" span: the foundation is now detached from $d^*/B=0.7$ to 0.9, but regains support at its right edge. As a result, the hogging M/M_o is reduced. With further increase of h, the foundation regains contact at its left edge as well (i.e., the left cantilever-type span disappears), and the hogging M/M_o is further reduced, while a sagging M/M_o (of the order of 1.3) can now be observed in the middle of the simply supported-type span ($d^*/B\approx 0.8$).

With the rupture outcropping close to the right edge of the foundation ($s=9$ m), neither diversion nor diffusion can be observed [Fig. 11(c)]. As in the previous cases, initially ($h=0.3$ m) p/q is only marginally altered. For $h=1.0$ m, the rupture then outcrops just underneath the right edge of the foundation, and the contact pressures are reduced at the two ends, without yet losing contact. Increasing h to 2.0 m leads to detachment from the soil at both edges, from $d^*/B=0$ to 0.1 (to maintain moment equilibrium of the foundation) and from 0.9 to 1.0 (because the soil moves away). Each unsupported span acts as a cantilever on "elastic" supports. As a result, the stressing is reversed with M/M_o reaching −3.9 (hogging). Further increase of h does not cause any appreciable change.

Fig. 12 summarizes the effect of s on foundation rotation $\Delta\theta$. In general, $\Delta\theta$ is largest for $s=5$ m ($\Delta\theta=9.1°$ at $h=2$ m). It is significantly less for $s=1$ m (4.4° at $h=2$ m), and even lower for $s=9$ m (1.1° at $h=2$ m). While in the first two cases $\Delta\theta$ increases with h, in the last one, where the foundation stays on the "footwall," $\Delta\theta$ remains constant at 1.1° for $h\geqslant 0.4$ m. This behavior is due to the geometry of fault crossing the foundation. After the rupture has outcropped ($h\geqslant 0.4$ m), the foundation reaches a stable equilibrium with an unsupported edge and no further displacement: it cannot further be affected by the downward movement of the hanging wall, as it is no longer in contact. In contrast, for $s=1$ and 5 m, the increase of h leads to several redistributions/mechanism changes and an almost linear increase of $\Delta\theta$ with h.

Effect of Surcharge Load q

Focusing on the effect of q, we compare the response of a $B=10$ m practically rigid (EI$=10^8$ kNm^2) foundation positioned at $s=1$ and 9 m, subjected to $q=10$, 20, 40, and 80 kPa.

Fig. 13, in combination with the upper part of Fig. 11, summarize the comparison in terms of deformed mesh with shear strain contours for $h=2.0$ m. For $s=1$ m, the increase of q causes a more pronounced diversion of the rupture path and reduced $\Delta\theta$

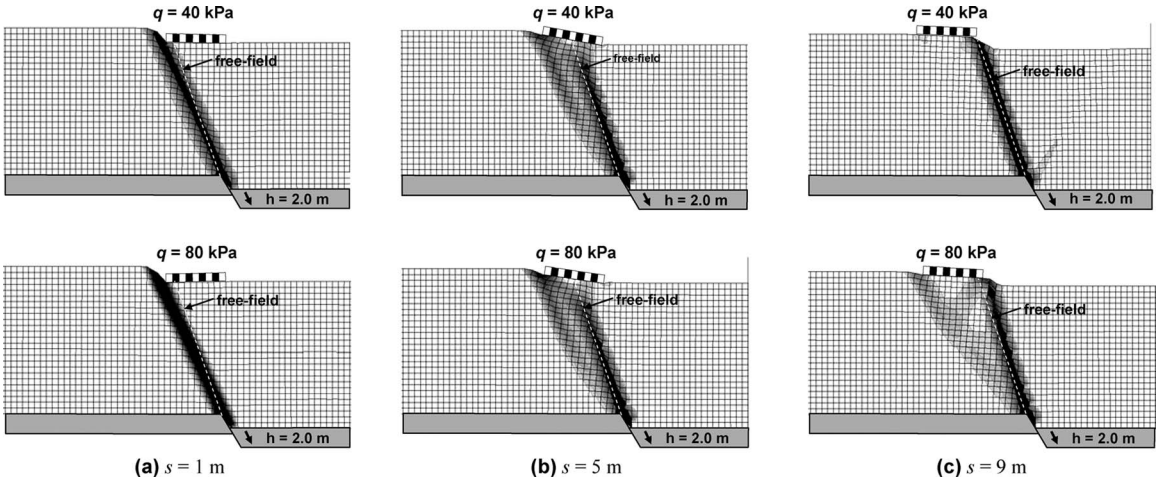

Fig. 13. Effect of distributed load q; $B=10$ m, EI$=10^8$ kN m^2 foundation: (a) $s=1$ m; (b) $s=5$ m; and (c) $s=9$ m; deformed mesh with shear strain contours, from top to bottom: $q=20$ kPa, $q=40$ kPa, and $q=80$ kPa

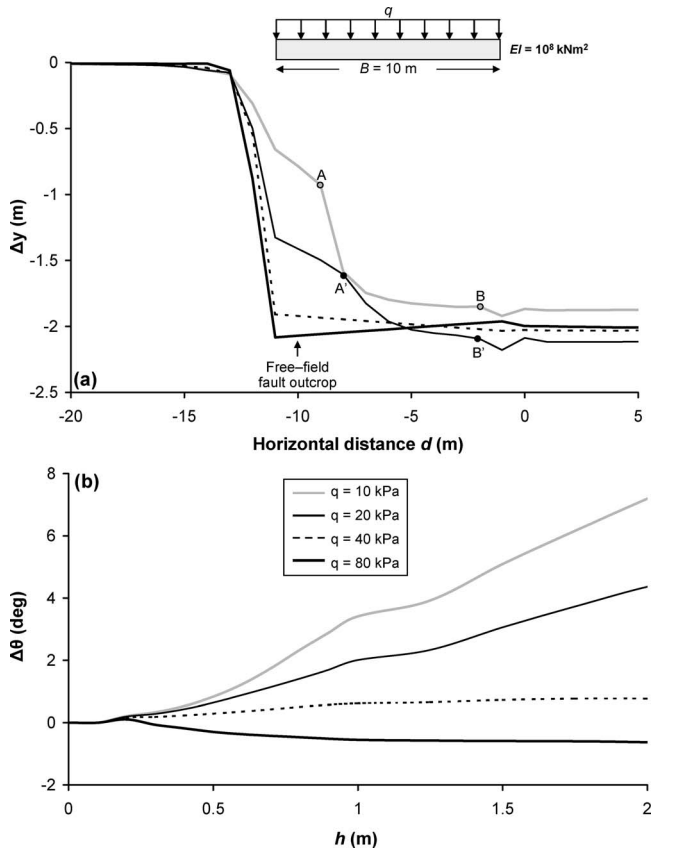

Fig. 14. Effect of foundation load q on the: (a) vertical displacement Δy at the soil surface (for $h=2$ m); (b) foundation rotation $\Delta\theta$ with respect to bedrock displacement, h; $B=10$ m, EI$=10^8$ kN m^2 foundation, unperturbed fault rupture emerging 1 m from the left edge of the foundation ($s=1$ m)

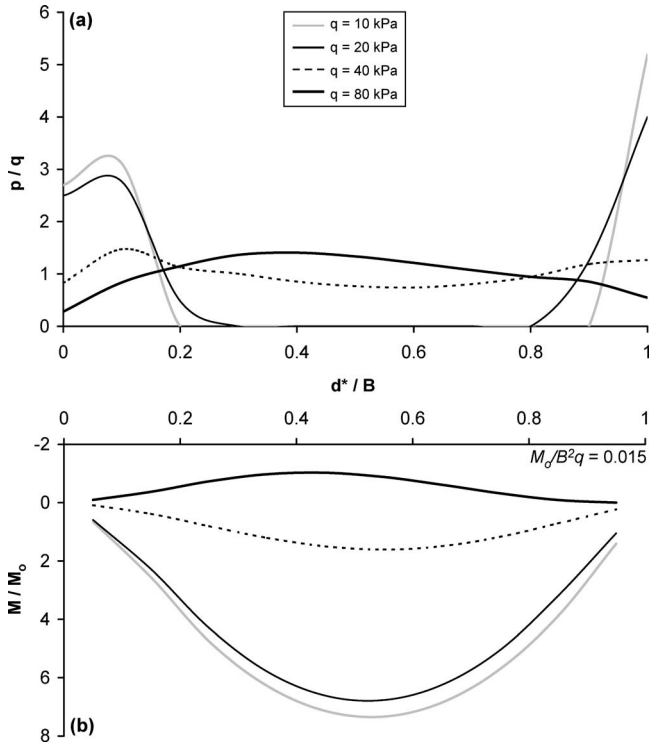

Fig. 15. Effect of distributed load q on the: (a) normalized contact pressure p/q; (b) normalized bending moment M/M_o (M_o: maximum bending moment, at $h=0$), for $h=2$ m; $B=10$ m, EI$=10^8$ kN m^2 foundation, unperturbed fault rupture emerging 1 m from the left edge of the foundation ($s=1$ m)

[Figs. 11(a) and 13(a)]. The effect of q on Δy and $\Delta\theta$ is shown in Fig. 14. While with $q\leqslant 20$ kPa, the foundation is detached from the soil near the middle [from A to B, and from A′ to B′, for 10 and 20 kPa, respectively; Fig. 14(a)], $q=40$ kPa is enough to maintain full contact, and reduce $\Delta\theta$ significantly [Fig. 14(b)]. Interestingly, further increasing q to 80 kPa leads to reversal of $\Delta\theta$ (anticlockwise instead of clockwise), which now reaches $-0.6°$. This is because the increased surcharge load, in combination with the geometry of fault outcropping, generates a partial failure mechanism (sliding along the rupture zone). This mechanism overshadows the natural tendency of the foundation for clockwise rotation (since it is located on the hanging wall).

The effect of q on p/q and M/M_o is depicted in Fig. 15. While with $q=10$ kPa, the foundation separates from the soil for $d^*/B=$from 0.2 to 0.8, being supported only at the two edges, when $q\geqslant 40$ kPa full contact is maintained everywhere [Fig. 15(a)]. As a result, the maximum M/M_o is reduced significantly [Fig. 15(b)]. This decrease is highly nonlinear: while the difference between $q=10$ kPa and 20 kPa is only marginal, increasing q to 40 kPa diminishes M/M_o substantially. For $q=80$ kPa, M/M_o is reversed (reaching -1): *hogging* instead of *sagging*. While with lower surcharge loads ($q\leqslant 40$ kPa), the detachment at the center of the foundation is predominant (the generated M/M_o is mainly due to the centrally unsupported beam-type span of the foundation), with larger q the foundation is forced to maintain contact, and its behavior is dominated by loss of support at its left edge.

When the foundation is located centrally above the outcropping rupture in the free field [$s=5$ m; Figs. 11(b) and 13(b)], the increase of q induces a more pronounced accumulation of deformation along the secondary rupture (initiating from the left edge of the foundation). With $q\geqslant 40$ kPa, full contact is achieved everywhere. Foundation rotation $\Delta\theta$ is again decreased for larger values of q, but not as much as for $s=1$ m.

Finally, as shown in Figs. 11(c) and 13(c), for $s=9$ m (rupture close to the right edge of the foundation), the increase of q causes the development of a secondary rupture to the left of the foundation, clearly observable for $q=80$ kPa. It initiates at the left edge of the foundation and propagates downwards. Interestingly, a third antithetic shear zone also makes its appearance, initiating at the right edge. It can be claimed that with $q=80$ kPa, a bearing capacity type failure mechanism is partially activated because of lack of support by the faulting block.

Fig. 16 shows the effect of q on Δy and $\Delta\theta$. The increase of q implies suppression of the unsupported parts of the foundation [Fig. 16(a)]. While for $q\leqslant 20$ kPa, support is lost at the two edges (from A to B and C to D, and A to B′ and C′ to D, for 10 and 20 kPa, respectively), the increase of q to 40 kPa prevents detachment at the left end and increases the contact area at the right end (from C″ to D). Full contact is achieved with $q=80$ kPa. In Fig. 16(b), observe that: (i) because of bearing capacity failure, $\Delta\theta$ increases with q, contrary to the trends observed for $s=1$ and 5 m; (ii) $\Delta\theta$ increases almost linearly with h for small fault displacements ($h\leqslant 0.5$ m), but is hardly affected by further increase of h for lightly loaded foundations; and (iii)

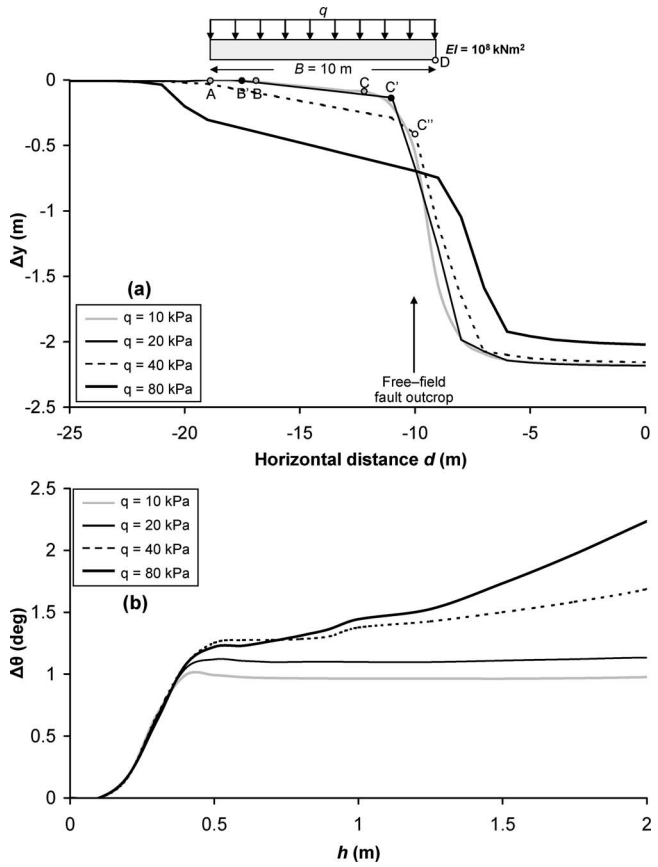

Fig. 16. Effect of distributed load q on the: (a) vertical displacement Δy at the soil surface (for $h=2$ m); (b) foundation rotation $\Delta\theta$ with respect to bedrock displacement h; EI$=10^8$ kN m^2 foundation, unperturbed fault rupture emerging 1 m from the right edge of the foundation ($s=9$ m)

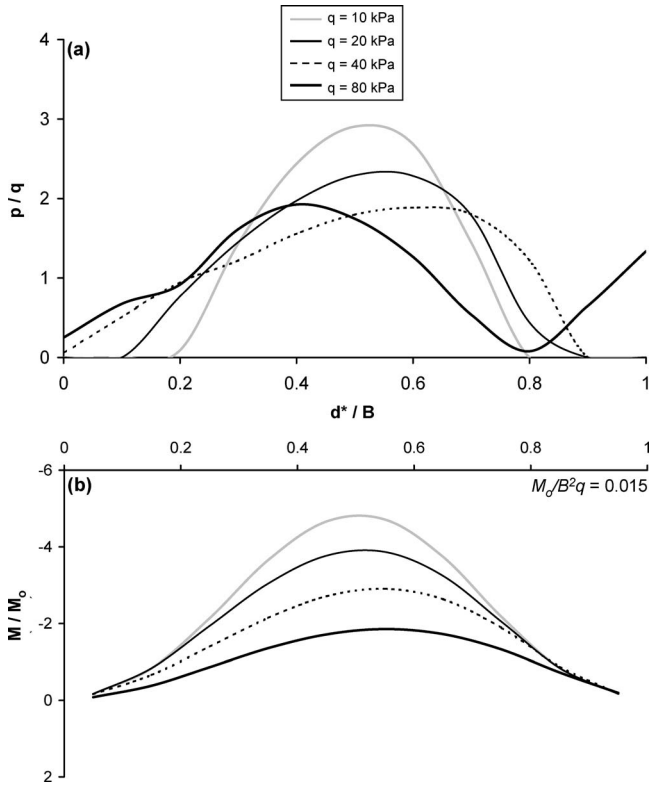

Fig. 17. Effect of foundation load q on the: (a) normalized contact pressure p/q; (b) normalized bending moment M/M_o (M_o: maximum bending moment, at $h=0$), for $h=2$ m; $B=10$ m, EI$=10^8$ kN m^2 foundation, unperturbed fault rupture emerging 1 m from the right edge of the foundation ($s=9$ m)

for larger q, $\Delta\theta$ is a little more sensitive to increases of h due to bearing capacity failure. The effect of q on p/q and M/M_o is depicted in Fig. 17.

Effect of Foundation Stiffness EI

Finally, to gain insight on the effect of EI, we compare the response of a $B=10$ m foundation with $q=20$ kPa at $s=5$ m, with EI$=10^4$, 10^7, and 10^8 kNm^2. As shown in Fig. 18(a), for this combination of q, B, and s, the response is not significantly affected by EI. The reduction of EI from 10^8 to 10^4 kNm^2 leads to almost no difference in p/q. An almost similar pressure distribution across the foundation implies that M does not vary significantly with EI. Indeed, the maximum $M=61$ kNm/m for EI$=10^8$ kNm^2, remains exactly the same for EI$=10^7$ kNm^2 (one order of magnitude difference), and is increased to 94 kNm/m for EI$=10^4$ kNm^2 (50% increase for three orders of magnitude difference in EI).

However, for the normalized M/M_o, the effect of EI is quite pronounced [Fig. 18(b)]. Although the distribution of M/M_o remains unaltered, the reduction of EI leads to increase of its maximum normalized value. Reducing EI from 10^8 to 10^7 kNm^2 (one order of magnitude) only leads to 40% increase of the maximum M/M_o. Further reduction of EI to 10^4 kNm^2 (three orders of magnitude) leads to 240% increase of the maximum normalized moment M/M_o. However, this increase is mainly due to the reduction of M_o and not to the increase of the tectonically induced M.

Limitations

The present study has certain limitations: (1) scale effects are incorporated in the FE model only in an approximate manner, as described in Anastasopoulos et al. (2007); and (2) both in the centrifuge and in the analysis, the sand is dry. In real conditions, the response may be altered due to transient pore water pressures for fast deformations or different effective stress conditions. Such issues are not addressed in this paper.

Conclusions

The main conclusions of this study are as follows:

1. The presented numerical methodology was validated through comparison of Class "A" predictions with results of centrifuge model tests. It predicted with reasonable accuracy: (a) the diversion and/or bifurcation of the outcropping dislocation; (b) the displacement profile at the ground surface; and (c) the rotation of the foundation.
2. The distress of the foundation stems mainly from loss of support due to detachment of its base from the soil. Proper modeling of soil-foundation contact is, thus, crucial. Depending on the position of the foundation on the outcropping fault

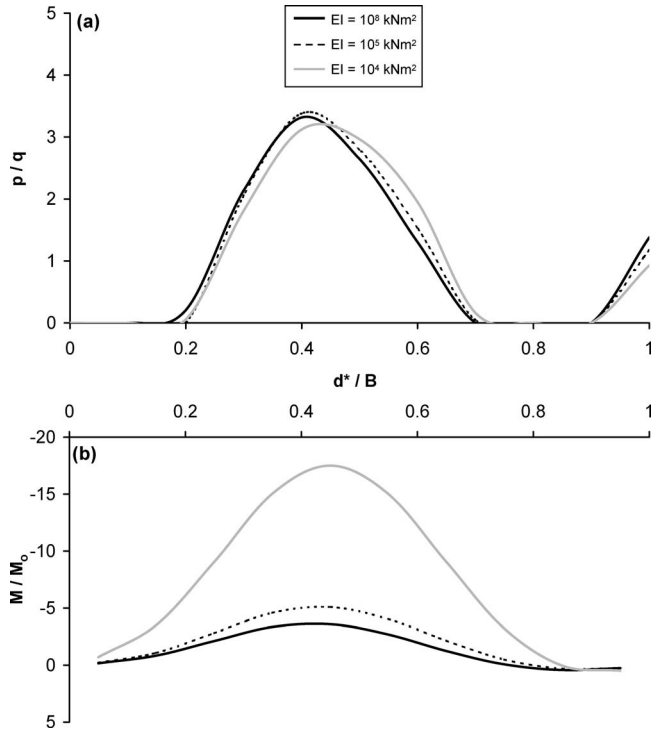

Fig. 18. Effect of foundation stiffness EI on the: (a) normalized contact pressure p/q; (b) normalized bending moment M/M_o (M_o: maximum bending moment, at $h=0$), for $h=2$ m; $B=10$ m foundation, $q=20$ kPa, unperturbed fault rupture emerging 5 m from the left edge of the foundation ($s=5$ m)

rupture, loss of support may take place either at the two ends or at the middle. In the former case, the unsupported span behaves as a cantilever on a central "elastic" support (giving hogging deformation), in the latter as a single span on "elastic" supports (sagging deformation).

3. In general, the increase of the surcharge load q decreases the width of the zone of separation, and, hence, the relative stressing of the foundation compared to the prefault loading is also decreased. The role of q is dual to this respect: (a) by pushing the foundation it compresses the soil, "flattening" any imposed anomalies; and (b) it changes the stress field underneath the structure, leading to diversion of the rupture. A "heavily" loaded foundation ($q>40$ kPa, for the cases examined herein) is capable of diverting the fault rupture and "flattening" the soil surface substantially.
4. Foundation rotation $\Delta\theta$ is a function of q and its position s relative to the free-field fault outcrop. When the rupture is near its far side (at the left), more heavily loaded foundations rotate less. With large surcharge loads ($q\geqslant 80$ kPa), the direction of $\Delta\theta$ may even be reversed due to generation of a partial failure mechanism (lack of support beneath the foundation due to the displacement of the hanging wall), which counterbalances the natural tendency for clockwise rotation into the hanging wall. When the rupture is close to the middle of the foundation, $\Delta\theta$ decreases with increasing q, but, the effect is not as pronounced. Finally, when the rupture is close to the right edge of the foundation, $\Delta\theta$ tends to increase with q. Moreover, $\Delta\theta$ is quite insensitive to the magnitude of fault offset h, beyond a value of 0.5 m, especially for low magnitudes of q.
5. The bending stiffness of the foundation EI does not have a significant effect. Δy, $\Delta\theta$, and p/q are all practically insensitive to EI, even for four orders of magnitudes difference in EI. Hence, the distribution of the bending moment M is also insensitive to EI. However, the maximum value of normalized bending moment, M/M_o, which represents the foundation loading ratio before and after faulting is affected by EI. However, this increase of M/M_o is mainly due to the reduction of the static M_o.

Acknowledgments

This work formed part of the EU research project "QUAKER," which is funded through the EU Fifth Framework Programme: Environment, Energy, and Sustainable Development, Research and Technological Development Activity of Generic Nature: the Fight against Natural and Technological Hazards, under Contract No. EVG1-CT-2002-00064. Partial support by OSE (the Greek Railway Organization) is also acknowledged.

References

ABAQUS. (2004). *ABAQUS V.6.4 user's manual*, Providence, R.I.

Ambraseys, N., and Jackson, J. (1984). "Seismic movements." *Ground movements and their effects on structures*, P. B. Attewell and R. K. Taylor, eds., Surrey Univ. Press, Surrey, U.K., 353–380.

Anastasopoulos, I. (2005). "Fault rupture-soil-foundation-structure interaction." Ph.D. thesis, School of Civil Engineering, National Technical Univ., Athens, Greece.

Anastasopoulos, I., Gazetas, G., Bransby, M. F., Davies, M. C. R., and El Nahas, A. (2007). "Fault rupture propagation through sand: Finite element analysis and validation through centrifuge experiments." *J. Geotech. Geoenviron. Eng.*, 133(8), 943–958.

Berill, J. B. (1983). "Two-dimensional analysis of the effect of fault rupture on buildings with shallow foundations." *Int. J. Soil Dyn. Earthquake Eng.*, 2(3), 156–160.

Bray, J. D. (1990). "The effects of tectonic movements on stresses and deformations in earth embankments." Ph.D. thesis, Univ. of California, Berkeley.

Bray, J. D. (2001). "Developing mitigation measures for the hazards associated with earthquake surface fault rupture." *Proc., Workshop on Seismic Fault-Induced Failures—Possible Remedies for Damage to Urban Facilities*, 55–79.

Bray, J. D., Seed, R. B., Cluff, L. S., and Seed, H. B. (1994a). "Earthquake fault rupture propagation through soil." *J. Geotech. Engrg.*, 120(3), 543–561.

Bray, J. D., Seed, R. B., and Seed, H. B. (1994b). "Analysis of earthquake fault rupture propagation through cohesive soil." *J. Geotech. Engrg.*, 120(3), 562–580.

Brune, J. N., and Allen, C. R. (1967). "A low-stress-drop, low magnitude earthquake with surface faulting. The imperial, California earthquake of March 4, 1966." *Bull. Seismol. Soc. Am.*, 57, 501–514.

Cole, D. A., Jr., and Lade, P. V. (1984). "Influence zones in alluvium over dip-slip faults." *J. Geotech. Engrg.*, 110(5), 599–615.

El Nahas, A., Bransby, M. F., and Davies, M. C. R. (2006). "Centrifuge modelling of the interaction between normal fault rupture and rigid, strong raft foundations." *Proc., Int. Conf. on Physical Modelling in Geotechnics*, 337–342.

Eurocode EC8. (1994). "Structures in seismic regions. Part 5: Foundations, retaining structures, and geotechnical aspects." Commission of the European Communities, Brussels.

Gaudin, C. (2002). "Experimental and theoretical study of the behavior of supporting walls: Validation of design methods." Ph.D. thesis, Laboratoire Central des Ponts et Chaussées, Nantes, France.

Horsfield, W. T. (1977). "An experimental approach to basement-controlled faulting." *Geol. Mijnbouw*, 56(4), 363–370.

Johansson, J., and Konagai, K. (2004). "Fault induced permanent ground deformations—Simulations and experimental verification." *Proc., 13th World Conf. on Earthquake Engineering* (DVD-ROM), Int. Assoc. of Earthquake Engineering.

Kelson, K. I., Kang, K.-H., Page, W. D., Lee, C.-T., and Cluff, L. S. (2001). "Representative styles of deformation along the Chelungpu Fault from the 1999 Chi-Chi (Taiwan) Earthquake: Geomorphic characteristics and responses of man-made structures." *Bull. Seismol. Soc. Am.*, 91(5), 930–952.

Lambe, T. W. (1973). "Predictions in soil engineering." *Geotechnique*, 23(2), 149–202.

Muir Wood, D. (2002). "Some observations of volumetric instabilities in soils." *Int. J. Solids Struct.*, 39, 3429–3449.

Muir Wood, D., and Stone, K. J. L. (1994). "Some observations of zones of localisation in model tests on dry sand." *Localisation and bifurcation theory for soils and rocks*, R. Chambon, J. Desrues, and I. Vardoulakis, eds., Balkema, Rotterdam, The Netherlands, 155–164.

Nakai, T., Muir Wood, D., and Stone, K. J. L. (1995). "Numerical calculations of soil response over a displacing basement." *Soils Found.*, 35(2), 25–35.

Pietruszezak, S. T., and Mroz, Z. (1981). "Finite element analysis of deformation of strain softening materials." *Int. J. Numer. Methods Eng.*, 17, 327–334.

Roth, W. H., Scott, R. F., and Austin, I. (1981). "Centrifuge modelling of fault propagation through alluvial soils." *Geophys. Res. Lett.*, 8(6), 561–564.

Sanford, A. R. (1959). "Analytical and experimental study of simple geologic structures." *Bull. Geol. Soc. Am.*, 70, 19–52.

Slemmons, D. B. (1957). "Geological effects of the Dixie Valley-Fairview Peak, Nevada earthquakes of December 16, 1954." *Bull. Seismol. Soc. Am.*, 47(4), 353–375.

Stone, K. J. L., and Muir Wood, D. (1992). "Effects of dilatancy and particle size observed in model tests on sand." *Soils Found.*, 32(4), 43–57.

Taylor, C. L., Cline, K. M., Page, W. D., and Schwartz, D. P. (1985). "The Borah Peak, Idaho earthquake of October 28, 1983—Surface faulting and other phenomena." *Earthquake Spectra*, 2(1), 23–49.

Walters, J. V., and Thomas, J. N. (1982). "Shear zone development in granular materials." *Proc., 4th Int. Conf. on Numerical Methods in Geomechanics*, Vol. I, 263–274.

White, D. J., Take, W. A., and Bolton, M. D. (2003). "Soil deformation measurement using particle image velocimetry (PIV) and photogrammetry." *Geotechnique*, 53(7), 619–631.

White, R. J., Stone, K. J. L., and Jewel, R. J. (1994). "Effect of particle size on localization development in model tests on sand." *Centrifuge 94*, C. F. Leung, F. H. Lee, and T. S. Tan, eds., Balkema, Rotterdam, The Netherlands, 817–822.